Minimum Energy Spike Randomization for Neurons

Ali Nabi, Mohammad Mirzadeh, Frederic Gibou, and Jeff Moehlis

Abstract— With inspiration from Arthur Winfree's idea of randomizing the phase of an oscillator by driving its state to a set in which the phase is not defined, i.e., the phaseless set, we employ a Hamilton-Jacobi-Bellman approach to design a minimum energy control law that effectively randomizes the next spiking time for a two-dimensional conductance-based model of noisy oscillatory neurons. The control is initially designed for the deterministic system through the numerical solution of the Hamilton-Jacobi-Bellman partial differential equation for the cost-to-go function, from which the minimum energy stimulus can be found; then its performance is investigated in the presence of noise. It is shown that such control causes a considerable amount of randomization in the timing of the neuron's next spike.

I. Introduction

Patients with Parkinson's disease typically suffer from involuntary tremors in their upper limbs. One proposed cause for these tremors is the pathological synchronization that occurs among the spiking neurons of the basal ganglia and the thalamus, regions of the brain that are responsible for motor control [1]. For those patients who do not respond to drug therapy, Deep Brain Stimulation (DBS) offers alternative treatment. In this FDA-approved surgical procedure, an electrode is implanted inside the patient's brain that injects high frequency current pulses into the motor-control region of the brain [2], [3]. The pulses are generated by a pacemaker-like device that is implanted in the patient's chest and connected to the electrode via wires running under the skin and along the patient's neck [4]. This method of treatment has been successful for many patients, and a working hypothesis is that DBS desynchronizes the pathologically synchronized motor control neurons. Researchers are now motivated to consider alternative stimuli that can achieve acceptable levels of desynchronization with less possible side-effects such as tissue damage or adaptation, and with less energy consumption.

Different control methods have been investigated and applied to various neural models in the past. Among these, feedback control and optimal control are more prominent. These methods are attractive from a clinical perspective in that the control stimulus is applied only when needed (characterized by the feedback signal) and in an optimal way (characterized by the optimality criteria). There are examples

A. Nabi, M. Mirzadeh, F. Gibou, and J. Moehlis are with the Department of Mechanical Engineering, University of California at Santa Barbara, Santa Barbara, CA 93106, USA. {nabi,m.mirzadeh}@engineering.ucsb.edu {fgibou,moehlis}@engineering.ucsb.edu

of these both on a single neuron level [5], [6], [7], [8], [9] and on a population level [10], [11], [12], [13], [14]. Other studies have also shown potential in desynchronizing a population of pathologically synchronized neurons [15], [16], [17], [18], [19].

In this article, we employ the idea proposed in [20] to randomize the phase of an oscillator by driving the state of the oscillator to a set in which the phase is not defined, i.e., the phaseless set. When in an oscillatory mode, the neuron generates periodic action potentials in the form of voltage spikes. As with any oscillatory system, a phase variable can be defined to characterize the evolution of the system states on the periodic orbit. With the idea of asymptotic phase [21], [22], the phase concept is extended to other points in the state domain that are not on the periodic orbit. This allows the definition of isochrons [21], which are lines of constant phase defined in the basin of attraction of the periodic orbit, each presenting the locus of all initial conditions that result in trajectories that asymptotically converge to the same point on the periodic orbit. These isochrons converge at the phaseless set which is on the boundary of the stable periodic orbit's basin of attraction.

The idea is that once the state of the system is at the phaseless set, it could, under the influence of the intrinsic background noise, be kicked onto a random isochron and spiral out to the periodic orbit and land at a different phase than what it would have been without the control application. As a proof of concept, Fig. 1 shows the voltage traces and spike time histogram for a neuron described by a two-dimensional reduction of the Hodgkin-Huxley model (more formally introduced in the next section) driven by 100 different realizations of zero-mean Gaussian white noise with variance $2D = 2$, and initialized at its phaseless point. It is seen that the noise can cause the next spike time for the neuron to be totally randomized.

This idea is employed in [23] to achieve desynchronization in minimum time using level set methods where an event-based strategy has been considered for the two-dimensional reduction of the Hodgkin-Huxley equations. The authors use a Hamilton-Jacobi-Bellman (HJB) formulation to design an optimal control law that would desynchronize a population in minimum time. Here we use a similar setup but solve for an optimal control that uses minimum energy instead. The minimum energy design of the controller is of clinical interest as it can result in longer battery life for neurostimulators.

The organization of the paper is as follows. We first describe the model used for the neuron in Section II. Then in Section III, we derive the HJB equation and, in Section IV, give a brief description of the essentials of the numerical
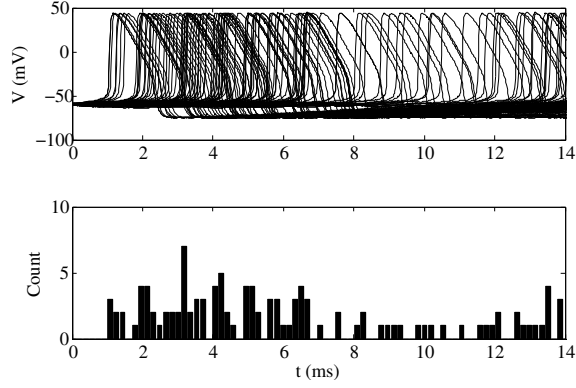
Fig. 1.   Voltage traces and spike time histogram for a two-dimensional reduction of the Hodgkin-Huxley model driven by 100 different realizations of a zero-mean Gaussian white noise with variance $2D = 2$, and initialized at its phaseless point.
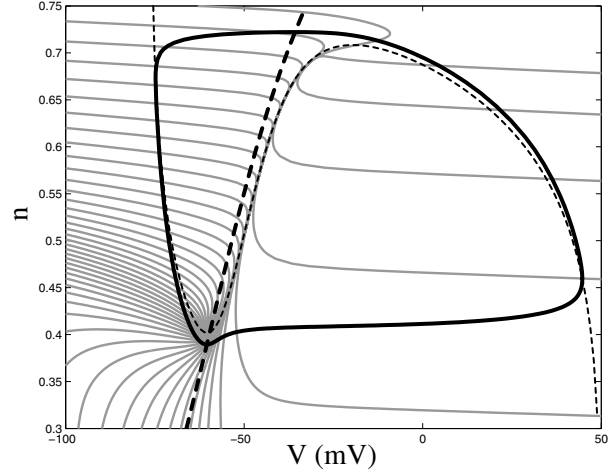
Fig. 2.   Periodic orbit (thick solid), V-nullcline (thin dashed), and n-nullcline (thick dashed), and fifty isochrons equally spaced in phase for the two-dimensional Hodgkin-Huxley model. The location of the unstable fixed point (phaseless point) for this system is at the intersection of the nullclines.

approach used to solve these equations. Results are presented and discussed in Section V. Finally, in Section VI some ongoing work is highlighted.

II. MODEL

We consider the two-dimensional reduced Hodgkin-Huxley model, analyzed, for example, in [24], [25]. In the absence of noise, this model is represented by the following equations:

$$
\begin{aligned}
\dot{V} &= (I_b + I(t) - \bar{g}_{Na}[m_\infty(V)]^3(0.8 - n)(V - V_{Na}) \\
&\quad - \bar{g}_K n^4(V - V_K) - \bar{g}_L(V - V_L))/c \,, \qquad (1) \\
\dot{n} &= a_n(V)(1 - n) - b_n(V)n \,,
\end{aligned}
$$

$$
\begin{aligned}
m_\infty(V) &= \frac{a_m(V)}{a_m(V) + b_m(V)} \,, \\
a_m(V) &= 0.1(V + 40)/(1 - \exp(-(V + 40)/10)) \,, \\
b_m(V) &= 4\exp(-(V + 65)/18) \,, \\
a_n(V) &= 0.01(V + 55)/(1 - \exp(-(V + 55)/10)) \,, \\
b_n(V) &= 0.125\exp(-(V + 65)/80) \,,
\end{aligned}
$$

$$
\begin{aligned}
V_{Na} &= 50 \text{ mV} \,, \ V_K = -77 \text{ mV} \,, \ V_L = -54.4 \text{ mV} \,, \\
\bar{g}_{Na} &= 120 \text{ mS/cm}^2 \,, \bar{g}_K = 36 \text{ mS/cm}^2 \,, \\
\bar{g}_L &= 0.3 \text{ mS/cm}^2 \,, \ c = 1 \ \mu\text{F/cm}^2.
\end{aligned}
$$

In this model, $V \in \mathbb{R}$ is the voltage across the neuron membrane and $n \in \mathbb{R}_{[0,1]}$ is the gating variable which corresponds to the state of the membrane's ion channels. $I_b \in \mathbb{R}$ is the baseline current, which represents the effect of other parts of the brain on the neuron under consideration and can be viewed as a bifurcation parameter that controls whether the neuron is in an excitable or an oscillatory regime. $I(t) : \mathbb{R} \mapsto \mathbb{R}$ is the stimulus current and $\bar{g}_{Na}$, $\bar{g}_K$, and $\bar{g}_L$ are the conductances of the sodium, potassium, and leakage channels, respectively. Also, V_{Na}, V_K, and V_L represent the

respective reversal potentials for these channels. $c \in \mathbb{R}^+$ is the constant membrane capacitance.

For this study, we consider $I_b = 10 \ \mu\text{A/cm}^2$ to ensure stable oscillatory (periodic spiking) behavior for the neuron. With this I_b, the period of spiking for the neuron is $T_s = 11.85$ ms. This oscillatory behavior is seen as a periodic orbit in the $V - n$ phase plane of the system, shown in Fig. 2 as the thick solid line. In the case of the present system, the phaseless point is the unstable fixed point [26]. The isochrons for the two-dimensional Hodgkin-Huxley system are shown in Fig. 2 as gray lines. As can be seen, these lines all converge at the unstable fixed point (or the phaseless point) where the $V-$ and $n-$nullclines intersect. By convention, the isochron that passes through the spiking point (maximum V) is the $\theta = 0$ isochron, where $\theta \in [0, 2\pi)$ is the phase of the neuron. The phase difference between every two neighboring isochrons in this figure is the same.

For simplicity, we rewrite (1) as

$$
\begin{aligned}
\dot{V} &= f_V(V, n) + u, \\
\dot{n} &= f_n(V, n),
\end{aligned} \qquad (2)
$$

where, $u = I(t)/c$ is the control input and

$$
\begin{aligned}
f_V &= (I_b - \bar{g}_{Na}[m_\infty(V)]^3(0.8 - n)(V - V_{Na}) \\
&\quad - \bar{g}_K n^4(V - V_K) - \bar{g}_L(V - V_L))/c, \qquad (3) \\
f_n &= a_n(V)(1 - n) - b_n(V)n
\end{aligned}
$$

are the state dynamics in the absence of external input. In the presence of noise, the system (2) is modified to

$$
\begin{aligned}
\dot{V} &= f_V(V, n) + \eta(t) + u, \\
\dot{n} &= f_n(V, n),
\end{aligned} \qquad (4)
$$

where the noise $\eta(t) = \sqrt{2D}\mathcal{N}(0,1)$ is a zero-mean white noise with variance $2D$. For the simulations presented in this article, we have taken $D = 1$.

The objective is to find the optimal control stimulus that, when applied to this system, drives the system to its phaseless set. As mentioned before, since the isochrons all emerge out from this point, the intrinsic background noise could then cause the system to fall on a random isochron, thereby randomizing the phase of the neuron. To this end, we first design the optimal control for the deterministic system (2) and analyze its performance when applied to the noisy system (4).

In order to achieve more stability in our numerical method described later, we scale down the V dimension in (2) by a factor of $K = 100$ so that the two states are of same order of magnitude. We note that this scaling is done only for the sake of numerical stability for the deterministic system. The results that we present are in the original $V - n$ coordinates. With the change of variables $z \equiv (x, y) = (\frac{1}{K}V, n)$, we get

$$\dot{z} = F(z) + Bu, \qquad (5)$$

where $B = [\frac{1}{K}, 0]^T$ and

$$F(z) = \left[\begin{array}{c} f_x(z) \\ f_y(z) \end{array} \right] = \left[\begin{array}{c} \frac{1}{K}f_V(Kx, y) \\ f_n(Kx, y) \end{array} \right]. \qquad (6)$$

III. OPTIMAL CONTROL

Consider the deterministic system (2). The objective is to find the minimum energy control law that would take the system to the phaseless set in some prespecified length of time $[0, T_{end}]$. The cost function that must be minimized is

$$J = \int_0^{T_{end}} u^2 dt + \gamma q(z(T_{end})), \qquad (7)$$

where $q(z(T_{end}))$ is the end point cost and γ is a penalizing scalar. We consider bounded inputs, i.e., $|u| \leq u_{max}$, to account for hardware and tissue endurance restrictions that are relevant in practice. Employing an HJB approach, we define the cost-to-go function (also known as the value function) from state z and time τ, for all $t \in [\tau, T_{end}]$, to be

$$\begin{aligned} \mathcal{V}(z(\tau), \tau) &= \min_{|u| \leq u_{max}} J \\ &= \min_{|u| \leq u_{max}} \left(\int_\tau^{T_{end}} u^2 dt + \gamma q(z(T_{end})) \right). \end{aligned} \qquad (8)$$

With this definition, following classical optimal control theory [27], we arrive at the well-known HJB equation

$$\begin{aligned} &-\frac{\partial \mathcal{V}}{\partial \tau}(z(\tau), \tau) = \\ &= \min_{|u| \leq u_{max}} \left[u^2 + \left(\frac{\partial \mathcal{V}}{\partial z}(z(\tau), \tau) \right)^T (F(z(\tau)) + Bu(\tau)) \right], \end{aligned} \qquad (9)$$

with the boundary condition

$$\mathcal{V}(z(T_{end}), T_{end}) = \gamma q(z(T_{end})). \qquad (10)$$

One can write (9) as

$$\frac{\partial \mathcal{V}}{\partial t} + \min_{|u| \leq u_{max}} \mathcal{H}(z, \nabla \mathcal{V}, u) = 0, \qquad (11)$$

where

$$\mathcal{H}(z, \nabla \mathcal{V}, u) = u^2 + (\nabla \mathcal{V}(z(t), t))^T (F(z(t)) + Bu(t)), \qquad (12)$$

is the Hamiltonian for the system and $\nabla \mathcal{V}$ is the gradient of the value function with respect to z, i.e., $(\frac{\partial \mathcal{V}}{\partial x}, \frac{\partial \mathcal{V}}{\partial y})^T$. The optimal control that globally minimizes $\mathcal{H}$ is obtained as

$$u^*(t) = \underset{|u| \leq u_{max}}{\arg\min} [u^2 + (\nabla \mathcal{V}(z^*(t), t))^T (F(z^*(t)) + Bu(t))], \qquad (13)$$

which yields

$$\begin{aligned} u^*(t) &= -\frac{1}{2K}\nabla_x \mathcal{V} & |\nabla_x \mathcal{V}| \leq 2Ku_{max}, \\ u^*(t) &= -\text{sign}(\nabla_x \mathcal{V})u_{max} & |\nabla_x \mathcal{V}| > 2Ku_{max}, \end{aligned} \qquad (14)$$

where $z^*(t)$ represents the optimal trajectory and $\nabla_x = \frac{\partial}{\partial x}$. With this optimal control, the Hamiltonian can be written as

$$\begin{aligned} \mathcal{H} &= \nabla \mathcal{V}^T F(z) - \frac{1}{4K^2}[\nabla_x \mathcal{V}]^2 & |\nabla_x \mathcal{V}| \leq 2Ku_{max}, \\ \mathcal{H} &= \nabla \mathcal{V}^T F(z) + u_{max}^2 - |\nabla_x \mathcal{V}|\frac{u_{max}}{K} & |\nabla_x \mathcal{V}| > 2Ku_{max}. \end{aligned}$$

IV. NUMERICAL APPROACH

In this section we briefly describe the numerical approach taken to solve the HJB equation. The HJB equation is special form of a broader class of partial differential equations (PDEs) known as the Hamilton-Jacobi (HJ) equations which are generally written as,

$$\frac{\partial \mathcal{V}}{\partial t} + \mathcal{H}(t, z, \mathcal{V}, \nabla \mathcal{V}) = 0. \qquad (15)$$

These equations frequently appear in many different areas like optimal control theory, image processing and computational physics [27], [28], [29]. As such, a great body of work has been devoted to the development of the theory and the numerical algorithms required for solving these equations over the past decades. Some of the initial efforts and developments include the seminal works of Crandall and Lions [30], [31], and Osher and Sethian [32]. For a more complete list of references, one may consult standard texts such as [28] and [29].

Starting from given initial data, $\mathcal{V}(z, 0)$, the procedure for finding the solution, $\mathcal{V}(z, t)$, to the HJ PDE may at first seem trivial: At each time step, it is enough to evaluate the Hamiltonian function $\mathcal{H}$ and carry out a forward integration to find the function $\mathcal{V}(z, t)$ at the subsequent time step. The only issue here would be that the solution gradient, $\nabla \mathcal{V}(z, t)$, which is needed to evaluate the Hamiltonian, is not explicitly given, which may simply be fixed by incorporating a finite difference approximation to evaluate $\nabla \mathcal{V}$ on a grid.

Although this idea is conceptually correct, there are non-trivial challenges involved that cause such a simple approach, like the aforementioned, to fail and not provide correct or even convergent results. Without going into the details, which may be found in the appropriate articles and texts mentioned above, an accurate and convergent algorithm for solving the HJ equation consists of three separate steps.

1) **Computing the solution gradient:** If one starts from sufficiently smooth initial data $\mathcal{V}(z, 0)$, solutions to HJ equation are usually continuous but could have discontinuities in their gradients [28]. As a result, if simple, classical finite difference approaches are taken to evaluate the gradients, numerical solutions may show unphysical oscillations near these discontinuities which can even cause the numerical algorithm to diverge. A fix to this problem is to use the so-called "essentially non-oscillatory" (ENO) [33], [34] or "weighted essentially non-oscillatory" (WENO) [35] schemes for computing the gradient term. Although these are a subclass of finite difference methods, they are designed such that they do not produce oscillatory results when evaluating the gradients close to the discontinuities.

2) **Computing the Hamiltonian:** Once the gradients are computed through either ENO or WENO methods, the next step is to evaluate the Hamiltonian function. For linear problems, i.e., problems for which the Hamiltonian function is linear in $\nabla \mathcal{V}$, this is straightforward. However for nonlinear problems, special care must be taken to guarantee that "shocks" and "rarefactions" phenomena are well approximated. In particular, it is essential that the numerical method guarantees convergence to the correct viscosity solution. A simple evaluation of the Hamiltonian, $\mathcal{H}$, would lead to incorrect results. To address this problem the so-called "numerical" Hamiltonian function must be designed (see $\hat{\mathcal{H}}$ in [36]). The essence is to add the right amount of numerical dissipation (or viscosity) to avoid converging to an entropy violating solution, while avoiding excessive smearing of important features.

3) **Integrating in time:** Finally, once the Hamiltonian function is evaluated at each grid point, it is necessary to integrate the solution $\mathcal{V}(z, t)$ forward in time. Not every integration method is suitable for solving the semi-discrete HJ equation. Like before, a careless choice usually leads to oscillatory and even non-convergent result. Only a subclass of methods that have the "total variation diminishing" (TVD) property are suitable for this task [37], [38]. Similar to usual integration schemes, TVD schemes include methods from both Runge-Kutta and linear multistep families.

In this work we use the Level Set Methods Matlab toolbox developed by Ian Mitchell [39] and utilize a solver with the third-order accurate ENO method for discretizing the spatial gradients accompanied with a third-order accurate TVD Runge-Kutta time integration method to solve (11).
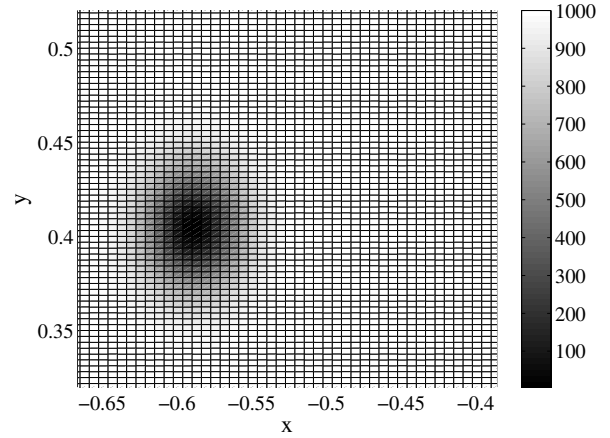

Fig. 3. The end point cost for the HJB equations on a 321×321 grid. Only the region around (x_{pl}, y_{pl}) of the domain is shown for better visualization. The value of the cost in the rest of the domain is 1000.

The numerical Hamiltonian is computed from the local Lax-Friedrichs (LLF) method.

We set $T_{end} = 7$ ms and use a 321×321 grid for the states (x, y) on a rectangular domain $-1 \leq x \leq 1$ and $0 \leq y \leq 1$ to solve the HJB equation (11) for the cost-to-go function $\mathcal{V}(z, t)$. The control bound is set to be $u_{max} = 10 \ \mu\text{A}/\mu\text{F}$. We also set the end point cost (10) to be

$$
\mathcal{V}(z(T_{end}), T_{end}) = \gamma \left(1 - e^{-\left(\frac{(x - x_{pl})^2}{\sigma_x^2} + \frac{(y - y_{pl})^2}{\sigma_y^2} \right)} \right),
\tag{16}
$$

where $\gamma = 1000$, $\sigma_x^2 = \sigma_y^2 = 0.001$, and $(x_{pl}, y_{pl}) = (\frac{1}{K} V_{pl}, n_{pl})$ where $K = 100$ and $(V_{pl}, n_{pl}) = (-59.6, 0.403)$ is the phaseless target point. This Gaussian end point cost function (shown in Fig. 3) has a minimum of zero at the phaseless point that encourages the evolution of the controlled system towards this point. We note that we solve the HJB equation backward in time and treat this end point cost as the initial condition for the equations.

Once the solution $\mathcal{V}(z, t)$ is computed, the optimal control is found as a function of the state at all time steps (see (14)). Given this data in time and space, we set the initial condition for the system (2) to be the spiking point $(V_0, n_0) = (44.8, 0.459) \equiv (V_s, n_s)$, and find the associated optimal control sequence $u(t)$ through forward integration of (2). A fourth order Runge-Kutta method is used for this integration. It should be noted that since the optimal control data is found on spatial grid points, an interpolation scheme is needed to obtain the input off grid points while the forward integration is carried out. A simple bilinear interpolation was found to be adequate in this study. This optimal control sequence is then applied to the noisy system (4) to evaluate its performance in randomizing the noisy neuron's spiking time. A second-order stochastic Runge-Kutta method [40] was selected to perform the forward integration in time for the stochastic system (4).
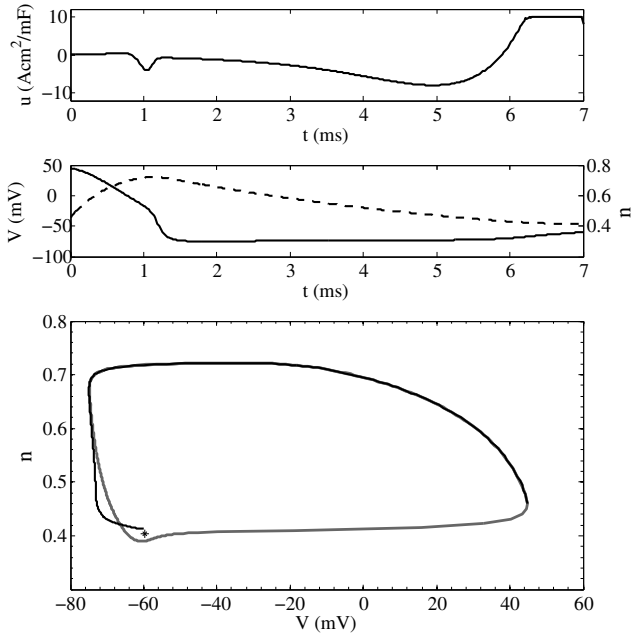
Fig. 4. Top: Minimum energy control law obtained for the deterministic single neuron system with the spiking point as the initial condition. The control is bounded to $|u| \leq 10 \ \mu A/\mu F$. Middle: the time evolution of the states of the system (V solid and n dashed). The starting point is the spiking state where $(V_s, n_s) = (44.8, 0.459)$ and the target point is the phaseless point where $(V_{pl}, n_{pl}) = (-59.6, 0.403)$. We see that the control is able to take the system close to the phaseless point. Bottom: the state space representation of the trajectory of the system under the control shown in top panel.
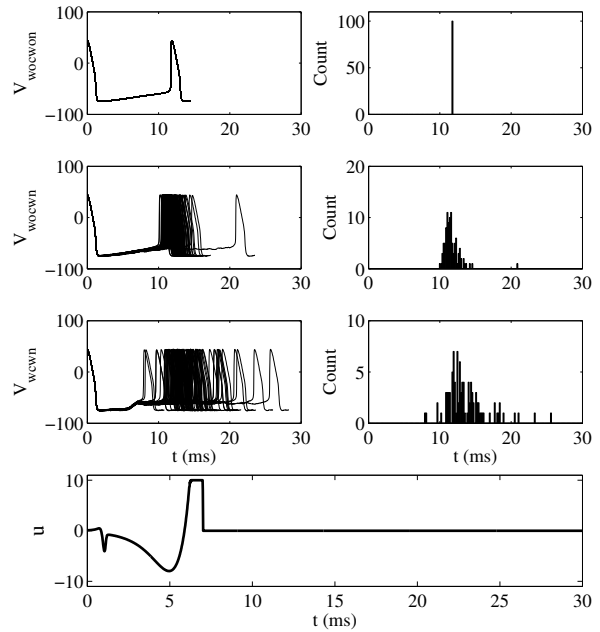
Fig. 5. Results for 100 different simulations for the system (2) with initial condition $(V_s, n_s) = (44.8, 0.459)$. First panel, voltage trace (left) and histogram (right) for the case of without noise and without external control; second panel, voltage trace (left) and histogram (right) for the case of 100 different noise realizations, without control; third panel: voltage trace (left) and histogram (right) for the case of 100 different noise realizations, with one cycle of control; fourth panel: the control input applied to the system. The input noise is $\eta = \sqrt{2D}\mathcal{N}(0, 1)$ with $D = 1$.

V. RESULTS AND DISCUSSION

The top panel in Fig. 4 shows the minimum energy control law for the deterministic neuron. We set the initial condition to be the spiking state as this is a practical observable which can be used as a trigger for the control, hence producing an event-based control. As can be seen in Fig. 4, the control has saturated at the bound value $u_{max} = 10 \ \mu A/\mu F$. Fig. 4 also shows the system trajectories in time and in the state space when driven by the control.

When the control shown in Fig. 4 is applied to the system in the presence of noise, it randomizes the next spiking instant of the neuron. Fig. 5 shows the results obtained for this case for 100 different numerical realizations. For comparison, we have included three different cases in this figure. The top panel shows the case where we have omitted both the noise and the control and have only considered the natural dynamics of the neuron. As expected, the neuron spikes at its natural period $T_s = 11.85$ ms for all 100 different trials. The second panel in Fig. 5 shows the case where noise is active, but the control is not. As can be seen, the spiking instant of the neuron varies due to the effect of different noise realizations. In the third panel, both noise and the control are acting on the neuron. We see that applying the control causes the next spiking instant of the neuron to

randomize over a considerable time interval. Finally, we note that the control has only been applied for one cycle as can be seen from the fourth panel in this figure. Fig. 6 shows the state space trajectories for these three cases. The dashed line shows the periodic orbit for the deterministic system without control. The light shade trajectories are those of the system with noise but without control. These trajectories follow the periodic orbit closely. The dark shade trajectories are for the case where both the noise and the control are applied. The phaseless point is shown with an asterisk marker.

VI. FUTURE WORK

The control found here can be applied to a population of pathologically synchronized neurons to desynchronize them by randomizing the phase of each neuron. In addition, one can include the states along the V-nullcline as part of the target set for the control algorithm as these points make a region in which the isochrons are densely populated [26]. If the state of the system is driven to this region, then, under the influence of noise, it can fall on either side of the V-nullcline resulting in different spike times.

REFERENCES

[1] J. Volkmann, M. Joliot, A. Mogilner, A. A. Ioannides, F. Lado, E. Fazzini, U. Ribary, and R. Llinàs, "Central motor loop oscillations in Parkinsonian resting tremor revealed magnetoencephalography," *Neurology*, vol. 46, no. 5, p. 1359, 1996.
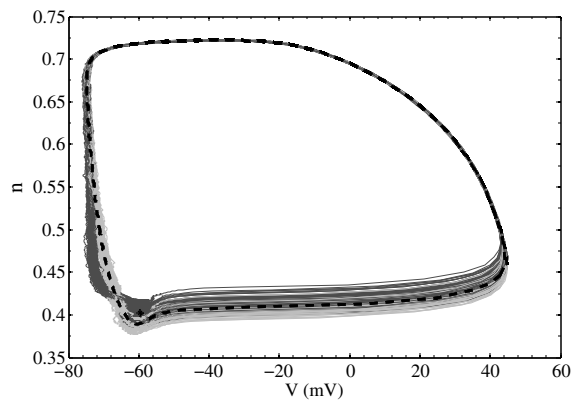
Fig. 6. The state space trajectories corresponding to the three cases shown in Fig. 5. The dashed, light shade, dark shade trajectories corresponds to the first, second, and third panels in Fig. 5, respectively. The asterisk marker, shows the location of the phaseless point. The input noise is $\eta = \sqrt{2D}\mathcal{N}(0,1)$ with $D = 1$.

[2] D. Pare, R. Curro'Dossi, and M. Steriade, "Neuronal basis of the Parkinsonian resting tremor: a hypothesis and its implications for treatment," *Neuroscience*, vol. 35, pp. 217–226, 1990.

[3] A. Nini, A. Feingold, H. Slovin, and H. Bergman, "Neurons in the globus pallidus do not show correlated activity in the normal monkey, but phase-locked oscillations appear in the MPTP model of Parkinsonism," *Journal of Neurophysiology*, vol. 74, no. 4, pp. 1800–1805, 1995.

[4] A. L. Benabid, P. Pollak, C. Gervason, D. Hoffmann, D. M. Gao, M. Hommel, J. E. Perret, and J. D. Rougemont, "Long-term suppression of tremor by chronic stimulation of the ventral intermediate thalamic nucleus," *The Lancet*, vol. 337, pp. 403–406, 1991.

[5] J. Moehlis, E. Shea-Brown, and H. Rabitz, "Optimal inputs for phase models of spiking neurons," *ASME J. Comp. Nonlin. Dyn.*, vol. 1, pp. 358–367, 2006.

[6] P. Danzl, A. Nabi, and J. Moehlis, "Charge-balanced spike timing control for phase models of spiking neurons," *Discrete and Continuous Dynamical Systems Series A*, vol. 28, pp. 1413–1435, 2010.

[7] A. Nabi and J. Moehlis, "Charge-balanced optimal inputs for phase models of spiking neurons," in *Proceedings of the 2009 ASME Dynamic Systems and Control Conference*, Hollywood, CA, 2009.

[8] ——, "Time optimal control of spiking neurons," *J. Math. Biol.*, 2011, DOI: 10.1007/s00285-011-0441-5.

[9] I. Dasanayake and J.-S. Li, "Optimal design of minimum-power stimuli for phase models of neuron oscillators," *Physical Review E*, vol. 83, p. 061916, 2011.

[10] P. A. Tass, *Phase Resetting in Medicine and Biology*. New York: Springer, 1999.

[11] O. V. Popovych, C. Hauptmann, and P. A. Tass, "Control of neuronal synchrony by nonlinear delayed feedback," *Biological Cybernetics*, vol. 95, no. 1, 2006.

[12] S. J. Schiff and T. Sauer, "Kalman filter control of a model of spatiotemporal cortical dynamics," *J. Neural Eng.*, vol. 5, pp. 1–8, 2008.

[13] S. J. Schiff, "Towards model-based control of Parkinson's disease," *Phil. Trans. R. Soc. A*, vol. 368, pp. 2269–2308, 2010.

[14] A. Nabi and J. Moehlis, "Single input optimal control for globally coupled neuron networks," *J. Neural Eng.*, 2011, DOI: 10.1088/1741-2560/8/6/065008.

[15] X. J. Feng, E. Shea-Brown, B. Greenwald, R. Kosut, and H. Rabitz, "Optimal deep brain stimulation of the subthalamic nucleus - a computational study," *Journal of Computational Neuroscience*, vol. 23, pp. 265–282, 2007.

[16] X. J. Feng, B. Greenwald, H. Rabitz, E. Shea-Brown, and R. Kosut, "Toward closed-loop optimization of deep brain stimulation for Parkinson's disease: concepts and lessons from a computational model," *J. Neural Eng.*, vol. 4, pp. L14–21, 2007.

[17] E. Schöll, G. Hiller, P. Hövel, and M. A. Dahlem, "Time-delayed feedback in neurosystems," *Phil. Trans. R. Soc. A*, vol. 367, pp. 1079–1096, 2009.

[18] A. Nabi and J. Moehlis, "Nonlinear hybrid control of phase models for coupled oscillators," in *Proceedings of the 2010 American Control Conference*, 2010.

[19] C. Wilson, B. Beverlin II, and T. Netoff, "Chaotic desynchronization as the therapeutic mechanism of deep brain stimulation," *Front. Syst. Neurosci.*, vol. 5, 2011.

[20] A. Winfree, *The Geometry of Biological Time, Second Edition*. New York: Springer, 2001.

[21] J. Guckenheimer, "Isochrons and phaseless sets," *J. Math. Biol.*, vol. 1, pp. 259–273, 1975.

[22] E. Brown, J. Moehlis, and P. Holmes, "On the phase reduction and response dynamics of neural oscillator populations," *Neural Comp.*, vol. 16, pp. 673–715, 2004.

[23] P. Danzl, J. Hespanha, and J. Moehlis, "Event-based minimum-time control of oscillatory neuron models," *Biol. Cybern.*, vol. 101, pp. 387–399, 2009.

[24] J. Moehlis, "Canards for a reduction of the Hodgkin-Huxley equations," *J. Math. Biol.*, vol. 52, pp. 141–153, 2006.

[25] J. Keener and J. Sneyd, *Mathematical Physiology*. New York: Springer, 1998.

[26] H. Osinga and J. Moehlis, "A continuation method for computing global isochrons," *SIAM Journal on Applied Dynamical Systems*, vol. 9, pp. 1201–1228, 2010.

[27] D. E. Kirk, *Optimal Control Theory: An Introduction*. New York: Dover Publications Inc., 1970.

[28] S. Osher and R. Fedkiw, *Level Set Methods and Dynamic Implicit Surfaces*, 1st ed. New York: Springer, 2003.

[29] J. A. Sethian, *Level Set Methods and Fast Marching Methods*, 2nd ed. Cambridge: Cambridge University Press, 1999.

[30] M. Crandall and P. Lions, "Viscosity solutions of Hamilton-Jacobi equations," *Transactions of the American Mathematical Society*, vol. 277, no. 1, pp. 1–42, 1983.

[31] M. G. Crandall and P. L. Lions, "Two approximations of solutions of Hamilton-Jacobi equations," *Mathematics of Computation*, vol. 43, no. 167, p. 1, 1984.

[32] S. Osher and J. A. Sethian, "Fronts propagating with curvature-dependent speed: algorithms based on Hamilton-Jacobi formulations," *Journal of Computational Physics*, vol. 79, no. 1, pp. 12–49, 1988.

[33] A. Harten, B. Engquist, S. Osher, and C. S. R., "Uniformly high order accurate essentially non-oscillatory schemes, III," *Journal of Computational Physics*, vol. 303, pp. 231–303, 1987.

[34] C. Shu and S. Osher, "Efficient implementation of essentially non-oscillatory shock-capturing schemes, II," *Journal of Computational Physics*, vol. 83, no. 1, pp. 32–78, 1989.

[35] X. Liu, S. Osher, and T. Chan, "Weighted essentially non-oscillatory schemes," *Journal of Computational Physics*, vol. 115, no. 1, pp. 200–212, 1994.

[36] S. Osher and C. Shu, "High-order essentially nonoscillatory schemes for Hamilton-Jacobi equations," *SIAM Journal on Numerical Analysis*, vol. 28, no. 4, pp. 907–922, 1991.

[37] C. Shu and S. Osher, "Efficient implementation of essentially non-oscillatory shock-capturing schemes," *Journal of Computational Physics*, vol. 83, no. 1, pp. 32–78, 1989.

[38] S. Gottlieb, C.-W. Shu, and E. Tadmor, "Strong stability-preserving high-order time discretization methods," *SIAM Review*, vol. 43, pp. 89–112, 2001.

[39] I. M. Mitchell, "A toolbox of level set methods," University of British Columbia, Tech. Rep. UBC CS TR-2007-11, 2007.

[40] R. L. Honeycutt, "Stochastic Runge-Kutta algorithms. I. white noise," *Physical Review A*, vol. 45, pp. 600–603, 1992.